Tunable perpendicular magnetoresistive sensor driven by shape and substrate induced magnetic anisotropy

Aleix Barrera Emile Fourneau Sergi Martín Josep Maria Batllori Jordi Alcalà Lluís Balcells Narcís Mestres Ngoc Duy Nguyen Alvaro Sanchez Alejandro V. Silhanek Anna Palau**

Dr. A. Palau
Insitut de Ciencia de Materials de Barcelona, CSIC, Campus de la UAB, 08193 Bellaterra, Catalonia, Spain
Email Address:palau@icmab.es
Prof. A.V. Silhanek
Solid-State Physics - Interfaces and Nanostructures, Q-MAT, CESAM, Université de Liège, B-4000 Sart Tilman, Belgium
Email Address:asilhanek@ulg.ac.be
A. Barrera, S. Martín, J. M. Batllori, J. Alcalà, Dr. Ll.Balcells, Dr. N. Mestres
Insitut de Ciencia de Materials de Barcelona, CSIC, Campus de la UAB, 08193 Bellaterra, Catalonia, Spain
E. Fourneau
Experimental Physics of Nanostructured Materials, Q-MAT, CESAM, Université de Liège, B-4000 Sart Tilman, Belgium
Solid-State Physics - Interfaces and Nanostructures, Q-MAT, CESAM, Université de Liège, B-4000 Sart Tilman, Belgium
Prof. N.D Nguyen
Solid-State Physics - Interfaces and Nanostructures, Q-MAT, CESAM, Université de Liège, B-4000 Sart Tilman, Belgium
Prof. A. Sanchez
Departament de Fisica, Universitat Autonoma de Barcelona, 08193 Bellaterra, Barcelona, Catalonia, Spain

Keywords: *magnetic materials, thin films, spintronics, magnetoresistance, magnetic sensors*

Control of magnetization reversal processes is a key issue to the implementation of magnetic materials in technological applications. The modulation of shape magnetic anisotropy in nanowire structures with high aspect ratio is an efficient way to tune sharp in-plane magnetic switching. However, control of fast magnetization reversal processes induced by perpendicular magnetic fields is much more challenging. Here, tunable sharp magnetoresistance changes, triggered by out-of-plane magnetic fields, are demonstrated in thin permalloy strips grown on single crystal substrates. Micromagnetic simulations are used to evaluate the resistance changes of the strips at different applied field values and directions and correlate them with the magnetic domain distribution. The experimentally observed sharp magnetic switching, tailored by the shape anisotropy of the strips, is properly accounted for by the numerical simulations when considering a substrate-induced uniaxial magnetic anisotropy. These results are promising for the design of magnetic sensors and other advanced magnetoresistive devices working with perpendicular magnetic fields by using simple structures.

1 Introduction

Precise control of magnetic domains and magnetization switching processes in ferromagnetic materials plays an essential role in emerging spintronic technologies. The possibility to induce sharp magnetic reversals at a given switching field has been the target of intense research because of their considerable potential for use in memory and sensing devices [1, 2]. Among many different approaches, the anisotropic magnetoresistance (AMR) effect has been widely used to detect the variation of micromagnetic configurations and reversal processes in a large variety of magnetic structures [3, 4, 5, 6]. In particular, magnetic sensing devices based on magnetoresistive effects have attracted large attention in the field of biosensing owing to its design simplicity, easy integration, and relatively large sensitivity as compared with other approaches [7].
Magnetoresistive sensors have generally been manufactured on structures with in-plane magnetic anisotropy. Sensing devices are usually patterned into stripes with high aspect ratio (nanorods or nanowires) to ac-

quire tunable magnetic properties due to their shape anisotropy [8, 9, 10]. However, the sensitivity of such devices is limited by their reduced effective sensing area, and complex structures involving multi-contact strip arrays, have to be used in order to enhance the sensor surface [11]. The development of perpendicular magnetoresistive devices considered of great technological relevance for sensing and memory applications, is much more challenging. Materials with perpendicular magnetic anisotropy may enable an effective solution although they usually require complicated multilayered stacks [12] or complex structures [8]. In particular, permalloy nanowires and films grown on specially patterned groove-substrates appear as a very powerful technique for single cell detection showing the highest sensitivity for out-of-plane magnetic fields [13, 14]. Here we investigate anisotropic magnetoresistance effects on a series of permalloy (Py) strips of different widths and thicknesses for applied magnetic fields perpendicular to the strip plane. Sharp anomalous peaks in the magnetoresistance curves are observed, indicative of an abrupt magnetization reversal mechanism. We show that the switching field where the abrupt magnetization reversal occurs can be tuned by controlling the shape anisotropy created through the width/thickness ratio. Different possible scenarios accounting for the observed effects such as external field misalignment or the existence of magnetic anisotropies are analyzed via micromagnetic simulations. Simulations and experiments indicate that the sharp magnetoresistance changes obtained at certain out-of-plane magnetic fields can be attributed to substrate-induced uniaxial magnetic anisotropy.

2 Results and discussion

Permalloy thin films of different thicknesses $t = 10 - 300$ nm were grown by sputtering on $LaAlO_3$ (LAO) single crystal substrates. Strips of different widths $w = 1 - 100$ μm and lengths $L = 100 - 200$ μm were fabricated by photolithography and lift-off techniques. Processing details can be found in the experimental section. **Figure 1**(a) shows a schematic representation of the transport measurement configuration along with a scanning electron microscopy (SEM) image of a Py strip of $t = 30$ nm and $w = 50$ μm. Figure 1(b) shows a schematic representation of Py strip arrays patterned for magnetic measurements and optical microscopy images of two arrays with strips of $t = 25$ nm $w = 10$ μm and 100 μm.

2.1 Magnetic Properties of permalloy thin films

Figure 2(a) shows the magnetization hysteresis loops for two Py un-patterned films of thickness $t = 10$ nm and 300 nm with in-plane (IP) and out-of-plane (OOP) applied magnetic field. For both films, the saturation occurs at much higher magnetic field for the OOP configuration ($\mu_0 H_s \sim 1000$ mT) than for the IP configuration, a clear sign of the dominant in-plane anisotropy imposed by the sample's geometry. Insets show magnetic force microscopy (MFM) images obtained for Py films of $t = 30$ nm and 300 nm. In the thinner film large in-plane magnetic domains are separated by Néel walls. Increasing the film thickness leads to an out-of-plane component of the mainly in-plane magnetization thus forming stripe domains separated by a Bloch-type domain wall.[15]
Figures 2(b) and (c) show a close look of IP and OOP hysteresis loops at low fields. The IP magnetization of the 10 nm film exhibits a very sharp square loop with a saturation field of $\mu_0 H_s \sim 1$ mT and a coercive field of $\mu_0 H_c \sim 0.5$ mT. The 300 nm film shows a nearly reversible linear decrease of the magnetization from its saturated value at $\mu_0 H_s \sim 25$ mT and a square loop at low fields with $\mu_0 H_c \sim 2.5$ mT. This magnetic response, typically observed in Py films above a critical thickness, has been ascribed to the presence of a perpendicular anisotropy favoring the formation of a stripe domain structure as revealed by magnetic-force microscopy images (see bottom inset of Figure 2(a)). For the OOP configuration (panel (c)), coercive fields of $\mu_0 H_c \sim 10$ mT and 1.5 mT are obtained for the 300 and 10 nm films, respectively. It is interesting to note the existence of a small hysteresis loop for the 10 nm-thick sample which could be attributed to either a small in-plane component of the applied field or the presence of an induced out-of-plane uniaxial anisotropy. The influence of the sample's width on the OOP hysteresis loop is analyzed in Figure 2(d) where we compare the low field hysteresis obtained for arrays of strips with $w = 10$ μm, $w = 100$ μm and an un-patterned film of the same thickness. We find that the coercive

field of the strips is higher than that of the un-patterned film and increases as w decreases. This trend, which will be further discussed in the following section, can be ascribed to demagnetizing effects.

2.2 Anisotropic magnetoresistance of permalloy strips

Magnetoresistance (MR) measurements are used to characterize the magnetic behaviour of patterned Py strips. According to the Anisotropic Magnetoresistance (AMR) effect, the electrical resistance of a monodomain magnetic structure depends on the orientation of the magnetization with respect to the current direction as follows [16]:

$$R(\varphi) = R_{\perp} + (R_{\parallel} - R_{\perp}) \sin^2 \varphi, \tag{1}$$

with $90° - \varphi$ being the angle between the magnetization and the current, while $R_{\perp}$ and $R_{\parallel}$ are the resistances when the magnetization is perpendicular ($\varphi = 0^o$) and parallel ($\varphi = 90^o$) to the current, respectively.

Figure 3(a) shows the variation of the magnetoresistance as a function of the angle θ, between the out-of-plane z direction and a 100 mT applied magnetic field as indicated in the sketches, obtained for a strip of thickness $t = 10$ nm and width $w = 5$ μm. Results for rotation parallel and perpendicular to the applied current direction are plotted. Nearly invariant resistance values are obtained for a wide range of angles, associated to a saturated IP magnetization which is either parallel ($R_{\parallel}^{ip} = 543$ Ω) or perpendicular ($R_{\perp}^{ip}$= 531 Ω) to the current. Sharp magnetoresistance peaks/dips appear close to θ= 0^o and 180^o, i.e. OOP, as a consequence of rapid magnetization rotation inside the sample plane resulting from the shape anisotropy.

Figure 3(b) shows the magnetoresistance curves obtained for the same strip by sweeping the applied magnetic field along the three principal directions defined by the sample geometry. i.e. magnetic field OOP, IP perpendicular to the current and IP parallel to the current (see insets and Figure 1(a)). The variation of the resistance for the different configurations of applied field can be associated to the AMR effect with a coherent rotation of the magnetization, considering that the mean angle between the current and the magnetization can be determined from the hysteresis loops according to the following equation[17]:

$$R(H) \propto [1 - (M(H)/M_{sat})^2], \tag{2}$$

where $M(H)$ is the magnetization for a given applied field and M_{sat} is the saturation magnetization. According to the hysteresis loops shown in Figure 2(a), the IP magnetoresistance (closed symbols) changes abruptly at the coercive field and corresponds to a maximum disorder of the magnetic domain distribution [18]. For the OOP configuration, a much smoother magnetoresistance variation is observed which can be associated to the wide hysteresis loop obtained for this configuration (open symbols in Figure 2(a)). Strikingly, for this particular configuration, in addition to the main magnetoresistance effect associated to a coherent magnetization rotation, two symmetrical abrupt magnetoresistance jumps appear at the switching field $\mu_0 H_{sw} \sim \pm 60$ mT. Similar jumps in the magnetoresistance have been reported in elongated ferromagnetic nanowires for IP magnetic field applied along its easy axis [9, 19], and attributed to a sharp switching of the magnetic moment due to a curling rotation [20, 21, 22, 23, 24].

In order to elucidate the nature of the MR jumps appearing in the Py strips we have systematically investigated the OOP magnetoresistance curves obtained for strips of different geometries.

Figure 4 shows the magnetic field dependence of the OOP magnetoresistance ratio $MR(\%) = (R(H)$-$R(0))\times 100/R(0)$, where $R(0)$ is the resistance at zero field and $R(H)$ the resistance in an external field H, obtained for a series of strips of different widths, w, with thicknesses $t = 10$ nm and 300 nm at 100 K. Abrupt MR changes of $\sim 0.2 - 1.6$ % are identified for all the strips. Similar MR curves are obtained at 200 K and 300 K (see Supporting Information Figure S1) although the MR value changes and, as expected, the value of H_{sw} decreases as the temperature increases. It is worth pointing out that the switching field where the magnetoresistance jumps occur lies in the range $\mu_0 H_{sw} \sim \pm$ 5 - 200 mT and strongly depends on the strip shape anisotropy.

Figure 5(a) shows the evolution of H_{sw}, with the strip width for samples of different thicknesses. H_{sw} is almost independent of the width for the strips with $t = 300$ nm whereas changes about one order of magnitude with increasing the strip's width from 1 to 100 μm in the case of thinner strips with $t = 10 - 30$ nm. We have included in the figure the coercive fields obtained from the hysteresis loops shown in Figure 2(d) for strips of $w = 10$ and 100 μm (star symbols) which are in good agreement with the $H_{sw}(w)$ dependence obtained from MR measurements. In Figure 5(b) the switching field H_{sw} is plotted as a function of w/t and shows a collapse of the datapoints onto a single trend indicating that demagnetization effects play an important role in determining the switching field.

2.3 Modelling of the anisotropic magnetoresistance

To gain a deeper understanding of the experimental results, we performed complementary micromagnetic and electrical transport simulations to evaluate the resistance change of the Py strips at different applied magnetic field values and directions. The modelled system consists of a ferromagnetic strip with saturation magnetization and exchange constant corresponding to conventional $Ni_{80}Fe_{20}$ alloy, absent of crystalline anisotropy and without any inhomogeneity or defect. The technical details concerning the micromagnetic simulation can be found in the Experimental section.
Figure 6(a) shows the magnetization hysteresis loops along the principal axis defined by the sample geometry (see inset of Figure 1(a)). Figure 6(b) shows the resulting AMR response and Figure 6(c) the sample's resistance as a function of angle for $\mu_0 H = 100$ mT.
The results of the simulations are in qualitative agreement with the experimental curves shown in Figures 2 and 3. However, for the OOP configuration (see green curves in Figure 3(b) and Figure 6(b)), the numerical findings fail to reproduce the abrupt magnetoresistance jumps observed experimentally. Such sharp resistance changes could be naturally accounted for by a sudden rearrangement of in-plane domains, with a disordered domain distribution at low fields switching to a $\hat{x}$-oriented domain distribution at high fields. Indeed, in thin films, the large demagnetization field in the $\hat{z}$ direction confines the magnetization to lie in the plane of the film. This is further confirmed in the inset of Figure 6(c) where the magnetization angle φ is plotted as a function of the magnetic field angle θ for 100 mT. The OOP component of the magnetization remains small ($< 5°$) irrespective of the value of θ, and is not correlated with the angular dependence of the sample's resistance. This reinforces the idea that the resistance changes observed during the OOP applied field sweeps are likely associated to a change of the IP magnetic domains arrangement.
In order to unveil the origin of this unexpected reversal of magnetization under OOP field, let us focus first on the switching mechanism for IP applied fields as obtained by the simulations. **Figure 7** shows a map of the magnetic domain distribution and associated variation of MR in $10 \times 3 \times 0.03$ μm samples at successive in-plane magnetic fields applied both perpendicular and parallel to the current direction. It can be observed that the switching mechanism consists of a buckling mode where the domains twist before flipping. At a high negative magnetic field, only one single domain exists and the strip resistance is minimal (maximal) for perpendicular (parallel) configuration. By increasing the field, the initial single domain progressively breaks into several domains with large components perpendicular to the applied field, leading to an increase (decrease) of the resistance. In the perpendicular case (Figure 7(a)), buckling domains are along the shape anisotropy axis and therefore are much more stable (visible between -5 and 3 mT) than for the parallel case (visible between 1 and 2 mT). A slight increase of magnetic field leads to the reversal of the magnetic domains with an abrupt change (reduction for perpendicular and increase for parallel case) of resistance.
In the following, we discuss two possible mechanisms leading to a fast in-plane rotation of the magnetization triggered by sweeping the OOP applied field.
Firstly, the sharp resistance change observed in the OOP magnetoresistance curves may arise from the existence of a small misalignment of the applied field, i.e. $\theta \neq 0°$ [25]. In this case, the magnetization reversal should occur for a magnetic field $H_{sw}^{OOP}(\theta) = H_{sw}^{IP} \sin^{-1}(\theta)$, where H_{sw}^{IP} is the in-plane coercive field. In order to explore this possibility, we simulated the MR response for different amplitudes of misalignment by tilting the applied field towards the direction of the current **(Figure 8**(a)) and per-

pendicular to it (Figure 8(c)). Simulations performed with a small in-plane component of the magnetic field (Figure 8(a)) show a clear jump of MR associated to a fast in-plane reversal of the magnetization, and for both configurations the calculated switching fields follow the expected angular dependence as displayed in the inset of panel (a). It is worth noting that the abrupt transition corresponds to an increase of resistance (domains align parallel to the current) in the case of a B_x component misalignment while the opposite is observed for a B_y component. This is consistent with the buckling mechanism as described for the IP magnetisation reversal in Figure 7.
For the sake of comparison, Figures 8(b) and (d) show the experimental MR curves measured under the same conditions. Results show two important differences. First, the predicted $\sin^{-1}(\theta)$ dependence is not observed in the experimental results (see inset of panel (b)). Secondly, in the case of a B_y component (Figure 8(d)), switching deeps are obtained instead of the peaks predicted by the numerical model in panel (c). This discrepancy between simulations and experiments suggests that an unwanted magnetic field misalignment does not provide a satisfactory explanation for the experimental results.
A possible alternative mechanism giving rise to an IP magnetization switching triggered by an OOP external magnetic field could be magnetic anisotropy, so far ignored in our model. While both *bcc* and *fcc* Py structures exhibit negligible magneto-crystalline anisotropy, Py thin films may exhibit an important perpendicular magnetic anisotropy (PMA). This induced magnetic anisotropy can be attributed to the internal stress coupled with non-zero magnetostriction coefficient and/or from columnar grains separated by nonmagnetic intergrain boundaries [26]. For films thicker than a critical thickness (around 200 nm), the stress-induced anisotropy overcomes the shape anisotropy and the PMA becomes visible as Py domains arrange themselves in stripes (as indeed seen in the bottom inset of Figure 2(a)). For films below the critical thickness, the shape anisotropy masks the effect of the induced uniaxial anisotropy but the latter is expected to be stronger as the stress-induced by the substrate tends to relax in thicker films. Indeed, the PMA is expected to evolve as t^{-2} for thin films [27]. For 50 nm-thick films or thinner, the anisotropy coefficient may be as high as K_{u1} =100 kJ/m^3 without leading to any nucleation of stripes domains because of the strong shape anisotropy. However, we postulate that an induced anisotropy can give rise to an IP magnetization reversal triggered by OOP magnetic field if the direction of the uniaxial anisotropic vector slightly deviates from the normal direction to the film. Such a slight deviation from the perfectly OOP case is possible notably because of misalignment between the sputtering source and the sample [28, 29, 30, 31] or due to the presence of stray field in the vicinity of the sputter head [32]. In addition, surface magnetic anisotropy and/or additional magnetostriction anisotropy may be induced at the interface between the Py film and substrate or a cap layer [33, 34].
To qualitatively illustrate how the magnetic anisotropy can account for the OOP AMR response observed experimentally, we will assume a uniaxial anisotropy with an easy-axis $\mathbf{u_k}$ in the x-z plane with an OOP angle β. The intensity of the associated anisotropy field H_k can be approximated by,

$$\mathbf{H_k} \simeq \frac{2K_{u1}}{\mu_0 M_s}(\mathbf{m}\cdot\mathbf{u_k})\mathbf{u_k} \tag{3}$$

with K_{u1} the anisotropy energy density. The IP component of the anisotropy field depends both on IP and OOP components of the magnetization,

$$H_{k,IP} = \frac{2K_{u1}\sin\beta}{\mu_0 M_s}[m_x\sin\beta + m_z\cos\beta]. \tag{4}$$

Therefore, for a positive applied field (and so $m_z > 0$), the IP effective field will favor domains aligned in the direction of $\mathbf{u_k}$ while the opposite is true for a negative OOP external field, leading to the possibility to induce an in-plane magnetization switch. In order to favour a magnetic reversal, the x-directed domains have to sustain an anisotropy field oriented in the opposite direction with a large enough intensity ($B \sim 1$ mT for the Py bars in this work). Based on Eq. (4) and assuming a zero in-plane coercive field, the anisotropy field is opposed to the IP magnetization if $m_z < 0$ and $|m_z/m_x| > \tan(\beta)$, which can be approximated by the condition $90° - \varphi > \beta$ with φ the magnetization angle with respect to the OOP direction.

An example is illustrated in **Figure 9**(a) corresponding to the simulated AMR signal of a 10 μm $\times$ 1 μm strip with a thickness of 30 nm and uniaxial magnetic anisotropy $K_{u1} = 120$ kJ/m^3 with an easy-axis forming an angle $\beta = 5.7°$ from the normal direction to the film. The associated in-plane magnetic domain distribution is shown for several selected applied magnetic fields. In this figure one can observe two sharp MR jumps symmetrically distributed around zero field, as the ones observed in the experiments, triggered by a perfectly aligned OOP magnetic field.
The switching field can be tuned through different properties of the device. In addition to the thickness and width of the stripe, it is influenced by the intensity and inclination of the induced uniaxial anisotropy. The panel (b) of Figure 9 shows the variation of the switching field for the same device as panel (a) but with different intensities of induced anisotropy. As expected from Eq. (4), H_{sw} decreases linearly with the anisotropy energy constant. Using $K_{u1} \simeq 125$ kJ/m^3, the computed switching field is close to the experimental value of 100 mT shown in Figure 5 for a magnetic bar of 1 μm wide. It is worth noting that this K_{u1} remains far from the maximal induced uniaxial anisotropy for a 30 nm-thick sample without stripes domain which is given by $K_{int} = 4\pi^2 A/t_{FM}^2 \simeq 500$ kJ/m^3 [27]. Interestingly, a reduction of the switching field and an increase of the MR are experimentally observed for thinner samples as shown in Figure 9(c), suggesting that the OOP is induced at the substrate interface. Moreover, the experimentally observed MR jumps are almost imperceptible in strips grown on silicon substrates (see Supporting Information Figure S2) providing further evidence of a substrate-induced magnetic anisotropy.
Figure 10(a) compares the experimental value of the switching field as a function of the misalignment angle (blue dots) with simulated values considering different intensity of uniaxal magnetic anisotropy. As discussed above, in the absence of any perpendicular magnetic anisotropy (red squares), the switching field at low tilted angles increase as $1/\theta$, leading to a huge discrepancy with experiments. However, when K_{u1} is around 100-120 kJ/m^3 (black and pink triangles), the predicted switching field saturates as θ tends to zero in agreement with experimental observations. Figure 10(b) shows the simulated magnetoresistance curves at different values of misalignment obtained for a device with $K_{u1} = 100$ kJ/m^3, corresponding to the black triangles of panel (a).
The origin of substrate-induced anisotropy may be associated to residual local stresses [34], dislocations [35], or associated to dipolar stray fields generated by a periodic modulated substrate [36, 37]. Indeed, atomic force microscopy images shown in **Figure 11** reveal that Py thin films reproduce the twinned structure of the LAO substrate with an out-of-plane tilting angle of $\sim$ 0.1-0.5 °. These images show large modulations of thickness ($\sim$ 20 nm) over scales of about 10 μm coexisting with a smaller scale periodic roughness ($\sim$ 1 nm) caused by the terraces in the LAO substrate. These features are absent in Si substrates where switching is negligible and therefore the magnetic uniaxial anisotropy could originate from a stress induced at the Py/LAO interface, enhanced by the natural structural modulations of LAO. Interestingly, the intensity of the stress-induced anisotropy can be tuned by adjusting the thickness whereas the angle can be controlled through the inclination of the sample during thin film deposition, forcing an oblique growth of the Py grains.

3 Conclusions

In summary, we have demonstrated the possibility to induce sharp in-plane magnetization reversals triggered by out-of-plane magnetic fields in permalloy strips on LAO substrates, producing large magnetoresitance changes (1 - 2 %) at tunable moderate applied fields (5 - 100 mT). Micromagnetic simulations have been implemented to elucidate the nature of the magnetoresistance jumps observed experimentally and suggest the existence of an important out-of-plane magnetic uniaxial anisotropy. The origin of this effect could be related to the transfer of the structural modulations on the substrate towards the Py film deposited on top. We are able to tailor the magnetic switching field by the shape anisotropy through the strip width-thickness ratio. These results may be relevant in a future generation of magneto-resistive sensors and functional devices working under perpendicular applied fields. φ

4 Experimental Section

Permalloy, $Fe_{20}Ni_{80}$, thin films of different thicknesses were deposited at room temperature by dc magnetron sputtering at a base pressure of 10^{-6} mbar and processing Ar pressure of $3{,}6.10^{-3}$ mbar on 5 mm $\times$ 5 mm $LaAlO_3$ and silicon substrates. A 2 nm capping protective layer of TiO_2 was deposited on the top of the thinner films to avoid oxidation. Strips of different widths were defined by photolithography and lift-off processes. Au contacts for 4-point contact transport measurements were deposited on top of the strips by sputtering. Magnetoresistance measurements were performed using a physical property measurement system (PPMS, Quantum Design) with the sample mounted on a goniometer permitting to change the relative orientation with respect to the applied magnetic field. Magnetization hysteresis loops of permalloy films and strip arrays were measured with a Quantum Design SQUID magnetometer with IP and OOP applied magnetic fields.
Micromagnetic simulations were performed using the open-source MuMax3 software for domain distribution calculations [38], and finite-element software COMSOL to compute the resistance change of the Py bars at different magnetic field intensities and directions. Due to computational limitations, simulations have been performed in structures with reduced dimensions compared to experimental devices. The length L was fixed to 10 µm while the width was optimized ($w = 4$ μm) in order to have the best compromise between maintaining the aspect ratio and avoiding large shape anisotropy for small w values. The IP micromagnetic cell dimensions were fixed to $10{\times}10$ nm^2 and the OOP size was set to 2.5, 5 and 10 nm for thickness of 10, 30 nm and thicker respectively. Calculations have been done using standard parameters for Py thin film M_s= 8.6×10^5 A/m and A_{ex}=13 pJ/m . The film is assumed to be free of magneto-crystalline anisotropy and thermal fluctuations are neglected. The four-point resistance has been calculated with voltage pads placed at a distance of 5% of the total length from the device edges.

Supporting Information
Supporting Information is available from the Wiley Online Library or from the author.

Acknowledgements
The authors acknowledge financial support from Spanish Ministry of Science and Innovation MCIN/ AEI /10.13039/501100011033/ through the "Severo Ochoa" Programme for Centres of Excellence in CEX2019-000917-S, HTSUPERFUN PID2021-124680OB-I00, co-financed by FEDER Una manera de hacer Europa, the Catalan Government with Grant 2017-SGR-1519, the EU COST action SUPERQUMAP CA21144, Fonds de la Recherche Scientifique - FNRS under the grants PDR T.0204.21 and CDR J.0176.22, and EraNet-CHIST-ERA R.8003.21, PCI2021-122028-2A and PCI2021-122083-2A. We also acknowledge the Scientific Services at ICMAB and the UAB PhD program in Materials Science. The authors thank J. Jazquez for fruitful discussions.

References

[1] C. Chappert, A. Fert, F. N. Van Dau, *Nature Materials* **2007**, *6* 813.

[2] J. Slaughter, *Annu. Rev. Mater. Res.* **2009**, *39* 277.

[3] T. Wren, O. Kazakova, *Journal of Applied Physics* **2015**, *117* 17E134.

[4] P. Perna, D. Maccariello, F. Ajejas, R. Guerrero, L. Méchin, S. Flament, J. Santamaria, R. Miranda, J. Camarero, *Advanced Functional Materials* **2017**, *27* 1700664.

[5] S. K. Vayalil1, A. Koorikkat, A. K. Gopi, S. V. Roth, P. S. A. Kumar, *Journal of Physics: Condensed Matter* **2020**, *32* 185804.

[6] M. Hayashi, L. Thomas, C. Rettner, R. Moriya, X. Jiang, S. S. P. Parkin, *Physical Review Letters* **2006**, *97* 207205.

[7] G. Lin, D. Makarov, G. Lin, O. G. Schmidt, *Lab on a Chip* **2017**, *17* 1884.

[8] H. T. Huang, T. R. Ger, Y. H. Lin, Z. H. Wei, *Lab on a Chip* **2013**, *13*, 15 3098.

[9] T. Y. Chung, S. Y. Hsu, *Journal of Applied Physics* **2008**, *103*, 7 18.

[10] V. D. Nguyen, L. Vila, P. Laczkowski, A. Marty, T. Faivre, J. P. Attané, *Physical Review Letters* **2011**, *107*, 13 1.

[11] D. Su, K. Wu, J. P. Wang, *Journal of Magnetism and Magnetic Materials* **2019**, *473* 484.

[12] J. S. Lee, J. Yoon, M. B. Kang, C. Y. You, *Journal of Magnetism and Magnetic Materials* **2014**, *358-359* 159.

[13] H. T. Huang, L. Ya-Hui, T.-R. Ger, Z.-H. Wei, *Applied Physics Express* **2013**, *6* 037001.

[14] H. T. Huang, T.-R. Ger, Z.-H. Wei, *Journal of Applied Physics* **2014**, *115* 17E518.

[15] D. B. J. Ben Youssef, N. Vukadinovic, M. Labrune, *Physical Review B* **2004**, *69* 174402.

[16] T. McGuire, R. Potter, *IEEE Transactions on Magnetics* **1975**, *11* 1018.

[17] W. Gil, D. Görlitz, M. Horisberger, J. Kötzler, *Physical Review B* **2005**, *72*, 13 134401.

[18] M. Viret, D. Vignoles, D. Cole, J. M. D. Coey, W. Allen, D. S. Daniel, J. F. Gregg, *Physical Review B* **1996**, *53*, 13 8464.

[19] S. N. Kozlov, O. V. Skryabina, S. V. Egorov, I. A. Golovchanskiy, A. A. Klimenko, K. S. Napolskii, V. S. Stolyarov, *Journal of Applied Physics* **2019**, *125* 063902.

[20] A. Aharoni, *Journal of Applied Physics* **1997**, *82*, 3 1281.

[21] L. Sun, Y. Hao, C. L. Chien, P. C. Searson, P. C. Searson, *IBM Journal of Research and Development* **2005**, *49*, 1 79.

[22] L. Van Thiem, L. T. Tu, M. H. Phan, *Sensors* **2015**, *15*, 3 5687.

[23] J. Zhang, S. Zhu, H. Li, L. Zhu, Y. Hu, W. Xia, X. Zhang, Y. Peng, J. Fu, *Nanoscale* **2018**, *10*, 21 10123.

[24] M. S. Sultan, *Physics Letters, Section A: General, Atomic and Solid State Physics* **2017**, *381*, 46 3896.

[25] H. Sato, R. Hanada, H. Sugawara, Y. Aoki, T. Ono, H. Miyajima, T. Shinjo, *Physical Review B* **2000**, *61*, 5 3227.

[26] S. Singh, H. Gao, U. Hartmann, *Physical Review B* **2018**, *98* 060414(R).

[27] J. McCord, B. Erkartal, T. von Hofe, L. Kienle, E. Quandt, O. Roshchupkina, J. Grenzer, *Journal of Applied Physics* **2013**, *113*, 7 073903.

[28] N. Eden, G. Kopnov, S. Fraenkel, M. Goldstein, A. Gerber, *Physical Review B* **2019**, *99*, 6 064432.

[29] Z. Ali, D. Basaula, K. Eid, M. Khan, *Thin Solid Films* **2021**, *735* 138899.

[30] B. Belyaev, A. Izotov, P. Solovev, *Physica B: Condensed Matter* **2016**, *481* 86.

[31] G. Wang, C. Dong, W. Wang, Z. Wang, G. Chai, C. Jiang, D. Xue, *Journal of Applied Physics* **2012**, *112*, 9 093907.

[32] M. Prutton, *Nature* **1962**, *193*, 4815 565.

[33] J. O. Rantschler, P. Chen, A. S. Arrott, R. D. McMichael, W. F. Egelhoff Jr, B. B. Maranville, *Journal of Applied Physics* **2005**, *97*, 10 10J113.

[34] U. Urdiroz, B.M.S.Teixeira, F. Palomares, J. Gonzalez, N. Sobolev, F. Cebollada, A. Mayoral, *AIP Advances* **2020**, *10*, 1 015013.

[35] G. Woltersdorf, B. Heinrich, *Physical Review B* **2004**, *69* 184417.

[36] M. Korner, K. Lenz, R. Gallardo, M. Fritzsche, A. Mucklich, Facsko, J. Lindner, P. Landeros, J. Fassbender, *Physical Review B* **2013**, *88* 054405.

[37] P. Vavassori, V. Metlushko, B. Ilic, M. Gobbi, M. Donolato, M. Cantoni, R. Bertacco, *Applied Physics Letters* **2008**, *93*, 20 10.

[38] A. Vansteenkiste, J. Leliaert, M. Dvornik, M. Helsen, F. Garcia-Sanchez, B. Van Waeyenberge, *AIP Advances* **2014**, *4*, 10 107133.

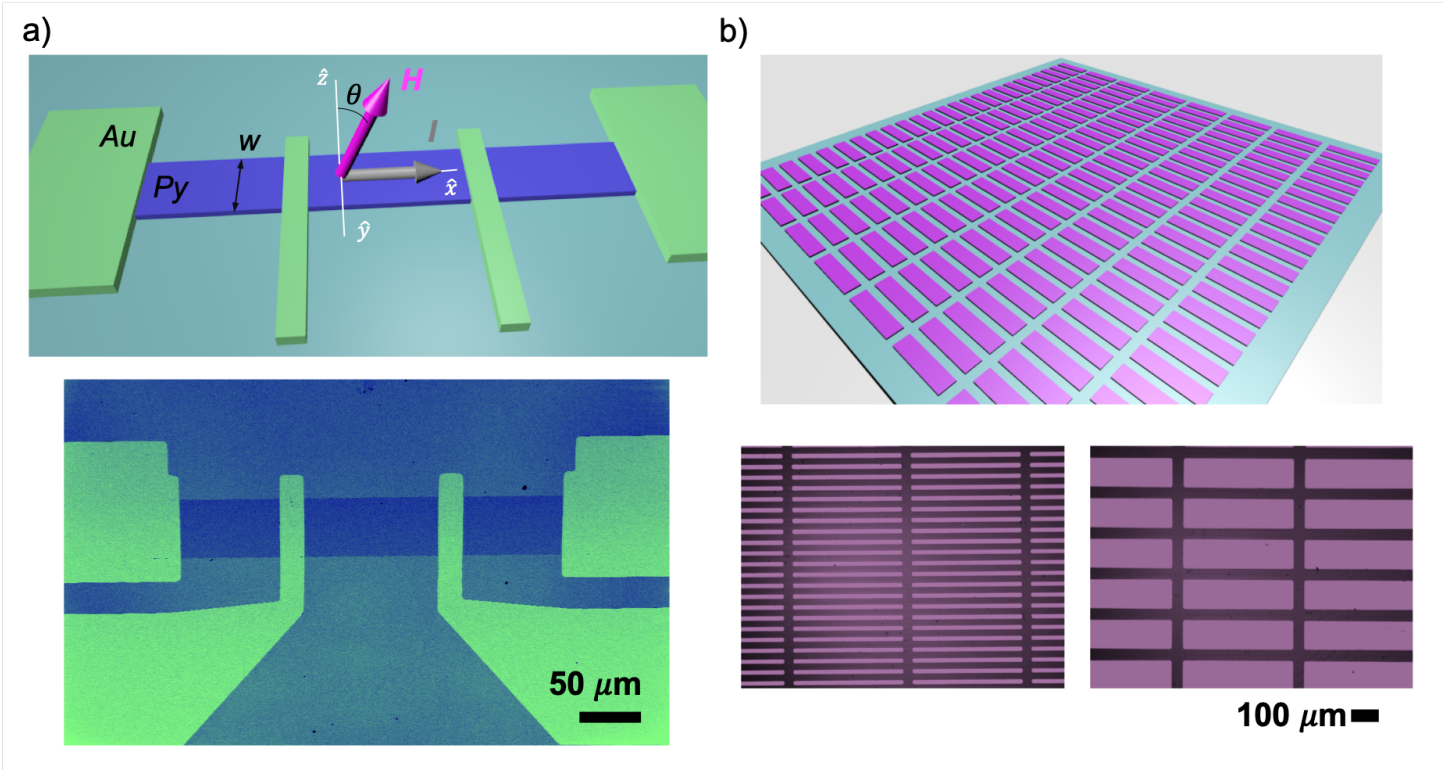

Figure 1: (a) Schematic of the transport measurement configuration with the main axis, current and magnetic field direction indicated (top) and SEM false-coloured images (bottom) of Py strip (blue) with four Au contacts (green) for transport measurements. (b) Schematic representation of patterned Py strip arrays (pink) for magnetization measurements (top) and optical images of two arrays with strips of widths $w = 10$ μm and 100 μm (bottom).

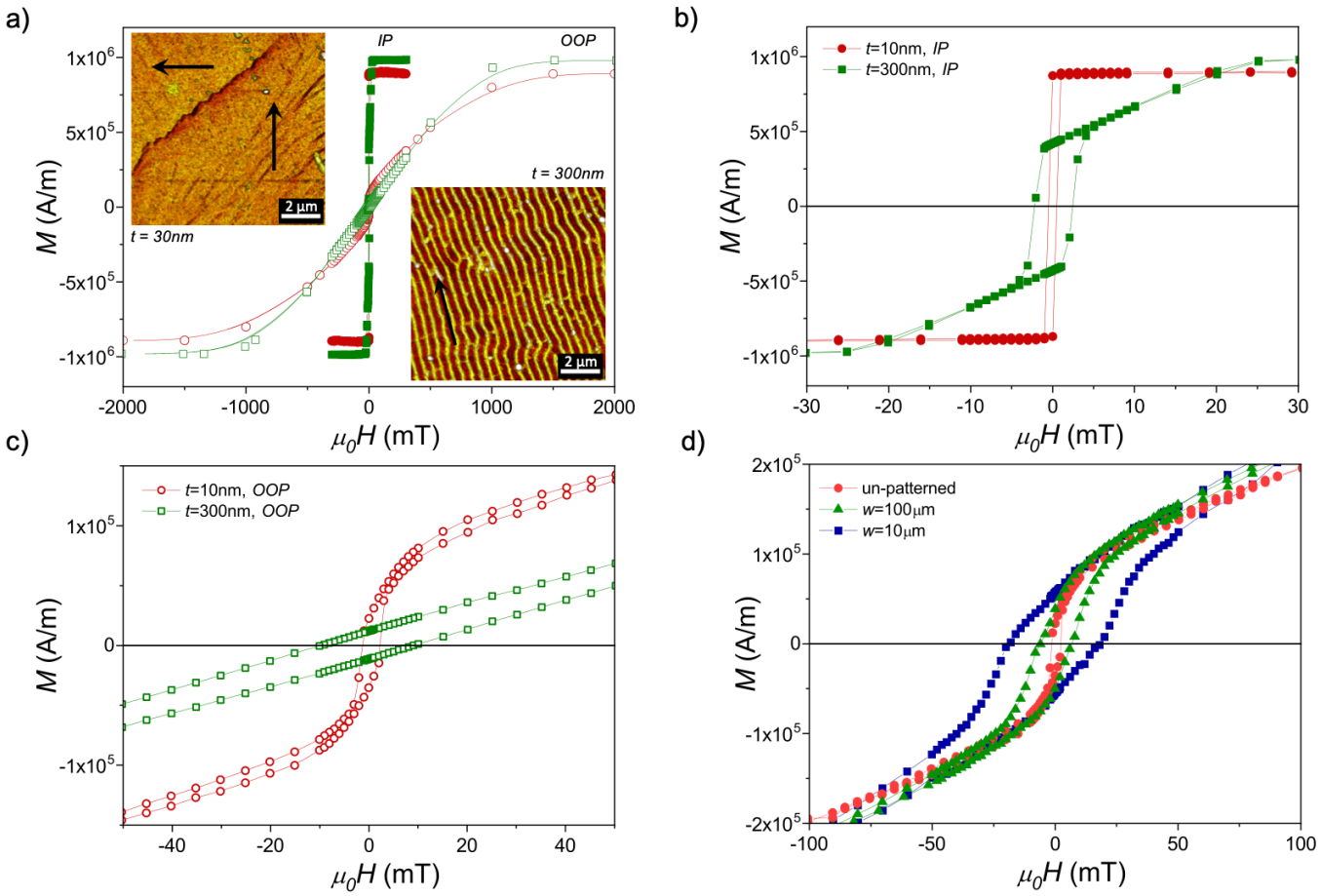

Figure 2: (a) Magnetization hysteresis loops measured at 100 K with IP (closed symbols) and OOP (open symbols) applied field for unpatterned Py films of $t = 10$ nm (red circles) and $t = 300$ nm (green squares). (b) and (c) Close looks of the IP and OOP loops at low fields, respectively. (d) OOP magnetization hysteresis loops for a 25 nm-thick un-patterned film (red circles), patterned array of strips with $w = 100$ μm (green triangles) and $w = 10$ μm (blue squares). Insets in (a) show MFM images obtained at room temperature for a 30 nm film (left top panel) and a 300 nm film (right bottom panel). Black arrows indicate the direction of magnetization.

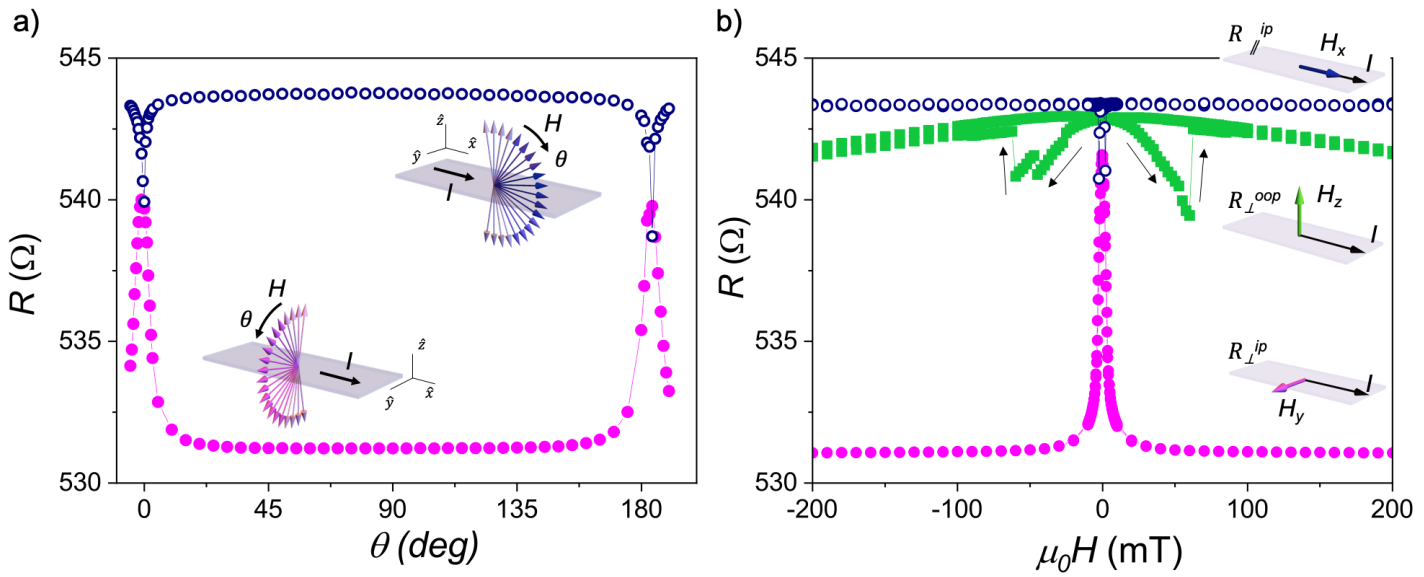

Figure 3: Anisotropic magnetoresistance of a Py strip of $t = 10$ nm and $w = 5$ μm measured at 100 K (a) by rotating an applied magnetic field of 100 mT in a plane parallel (blue open symbols) and perpendicular (pink closed symbols) to the current, as schematically shown on the sketches. (b) Magnetoresistance obtained for magnetic field sweeps along the three principal axes defined by the sample geometry: IP perpendicular to the current (closed pink circles), IP parallel to the current (open blue circles) and OOP (green squares), as indicated on the sketches. Arrows show the sweeping direction of the field for the OOP curve in the irreversible region.

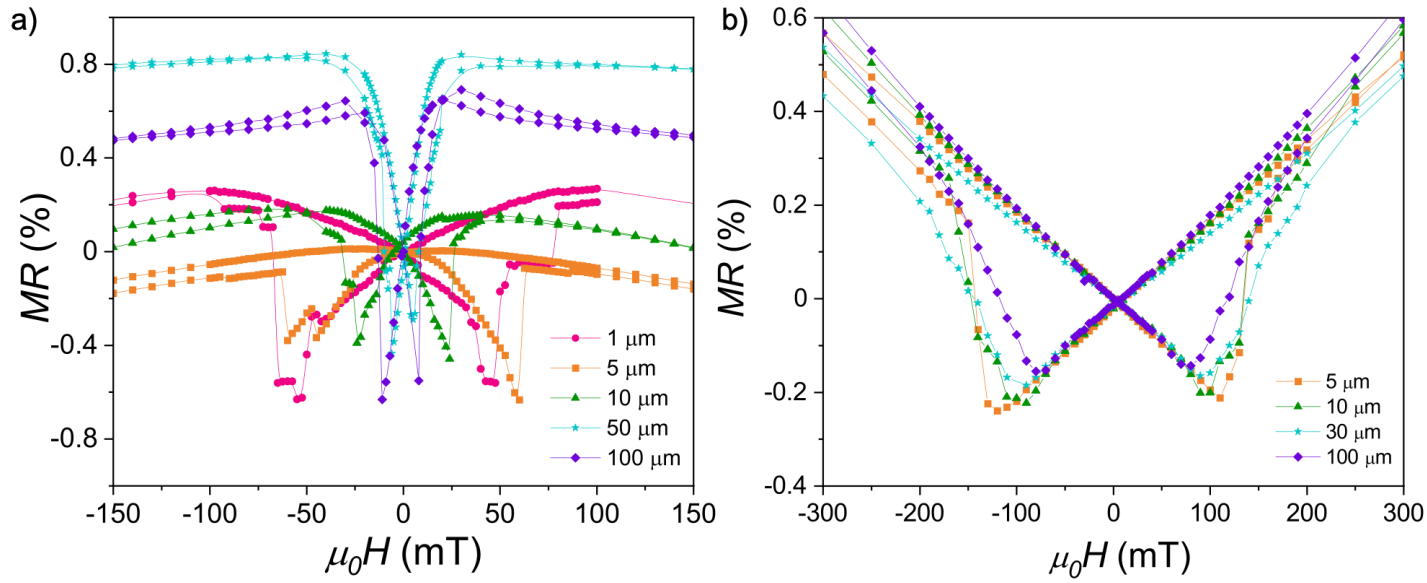

Figure 4: Magnetoresistance ratio as a function of the magnetic field applied OOP at 100 K for Py strips of different widths (indicated in the legend) and thicknesses (a) $t = 10$ nm and (b) $t = 300$ nm.

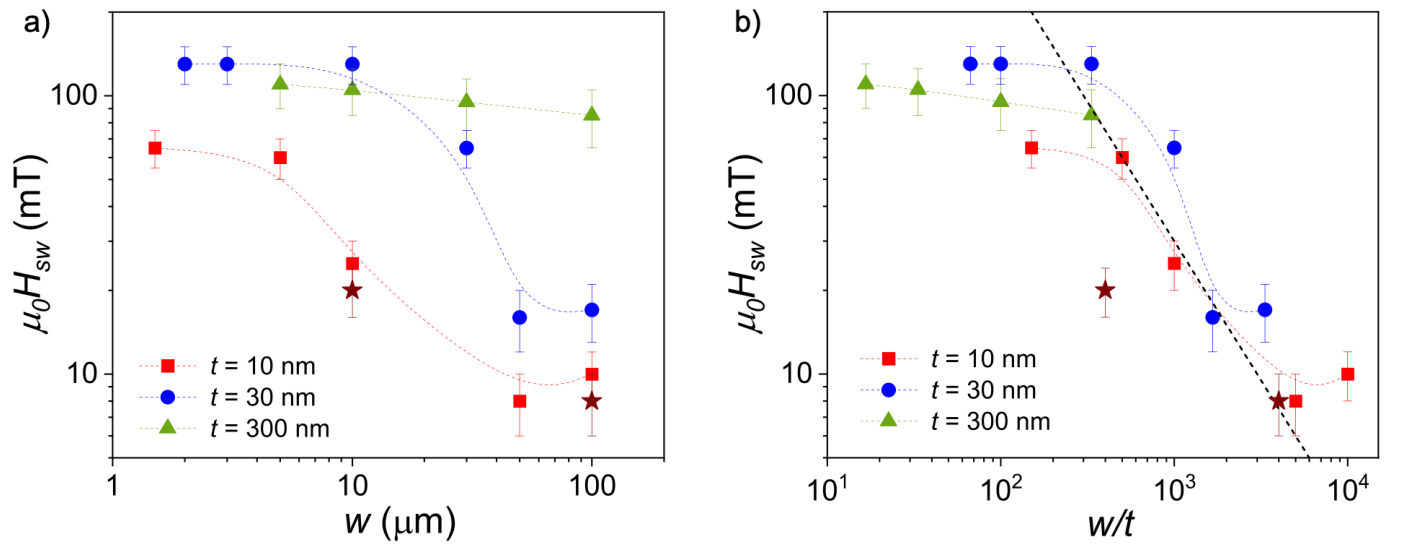

Figure 5: Switching field obtained for strips of different thicknesses as a function of the strip (a) width and (b) width/thickness ratio, in a log-log representation. The black dashed line in (b) shows a t/w dependence. Star shape symbols represent the coercive fields of two arrays of strips obtained through magnetization hysteresis loops.

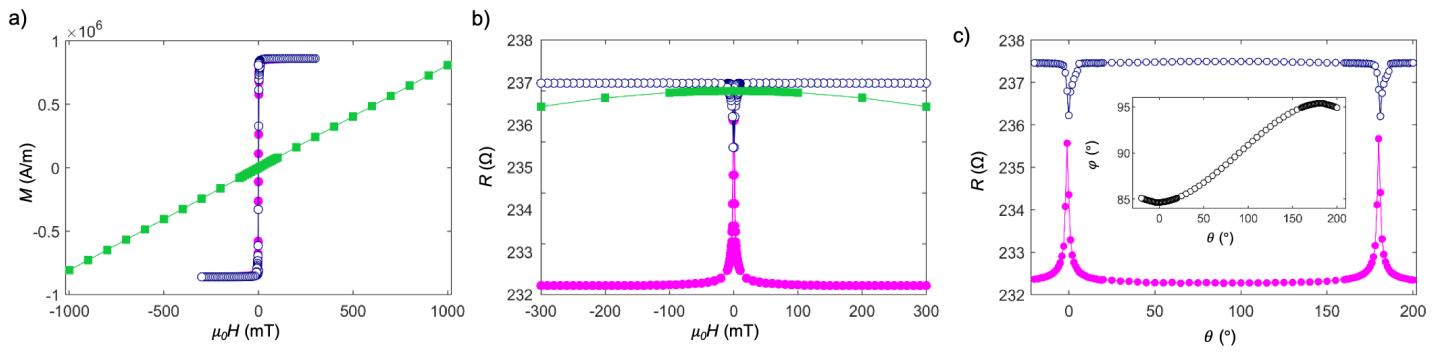

Figure 6: Micromagnetic simulations of (a) magnetization hysteresis loops and (b) associated magnetoresistance, calculated considering different applied magnetic field orientations (B_x (open blue circles), B_y (closed pink circles), B_z (green squares)). (c) Angular dependence of the magnetoresistance at fixed magnetic field of 100 mT tilted along the yz plane (closed symbols) and zx (open symbols). The inset shows the magnetization angle φ as a function of the magnetic field angle θ.

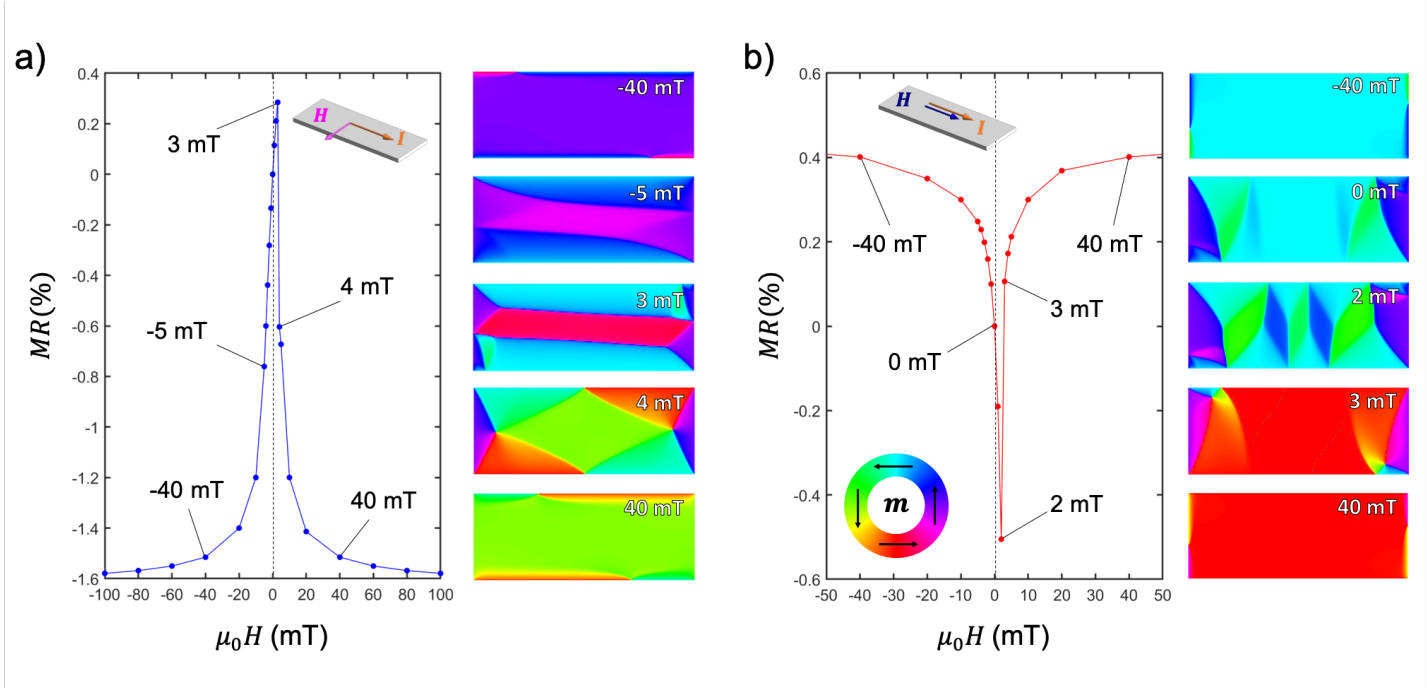

Figure 7: AMR response as a function of the magnetic field applied in-plane (a) perpendicular and (b) parallel to the applied current, along with the corresponding mapping of the magnetic domains distribution for a selected set of magnetic fields.

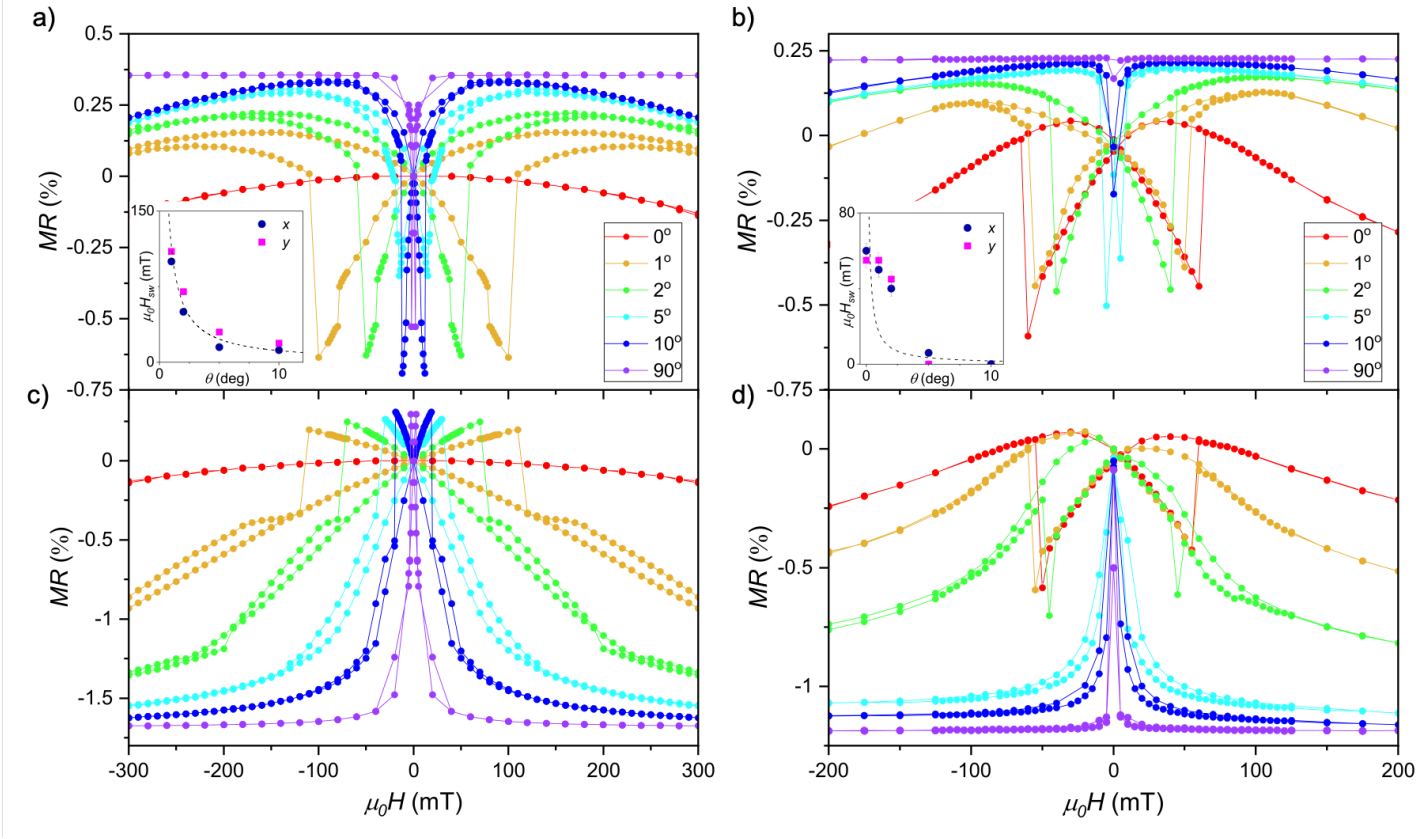

Figure 8: (a) and (c) Numerical simulations of the magnetoresistance for a device with $t = 30$ nm and $w = 4$ μm for an OOP applied field with a small misalignment angle θ towards and perpendicular to the direction of the current, respectively. (b) and (d) Experimental magnetoresistance curves measured for a strip of $t = 30$ nm and $w = 30$ μm at the same applied field conditions as (a) and (c), respectively. The insets in panel (a) and (b) show the computed and experimental switching fields as a function of the misalignment angle for tilting towards the x and the y axes. The dashed black lines correspond to a $\sin^{-1}(\theta)$ variation.

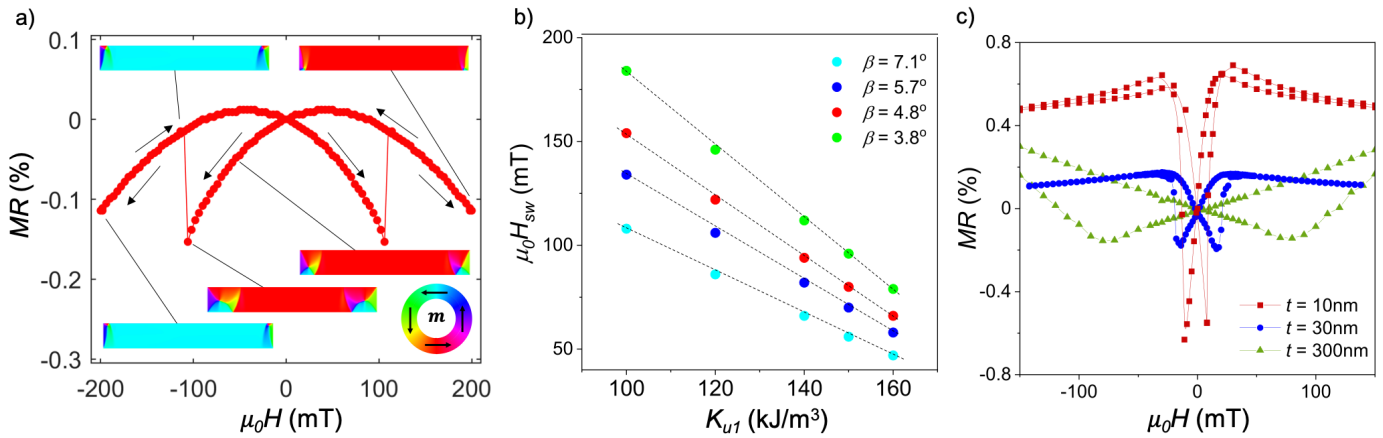

Figure 9: (a) Simulation of the magnetoresistance response of a 1-μm-wide and 30-nm-thick Py bars with tilted uniaxial anisotropy under perfectly OOP magnetic field. The arrows show the magnetic field sweep direction. The color maps represent the in-plane component of domains for a selection of magnetic fields during the descending sweep. (b) Variation of the switching field with the anisotropy vector direction and intensity. (c) Magnetoresistance curves measured for Py strips of $w = 100$ μm and different thicknesses.

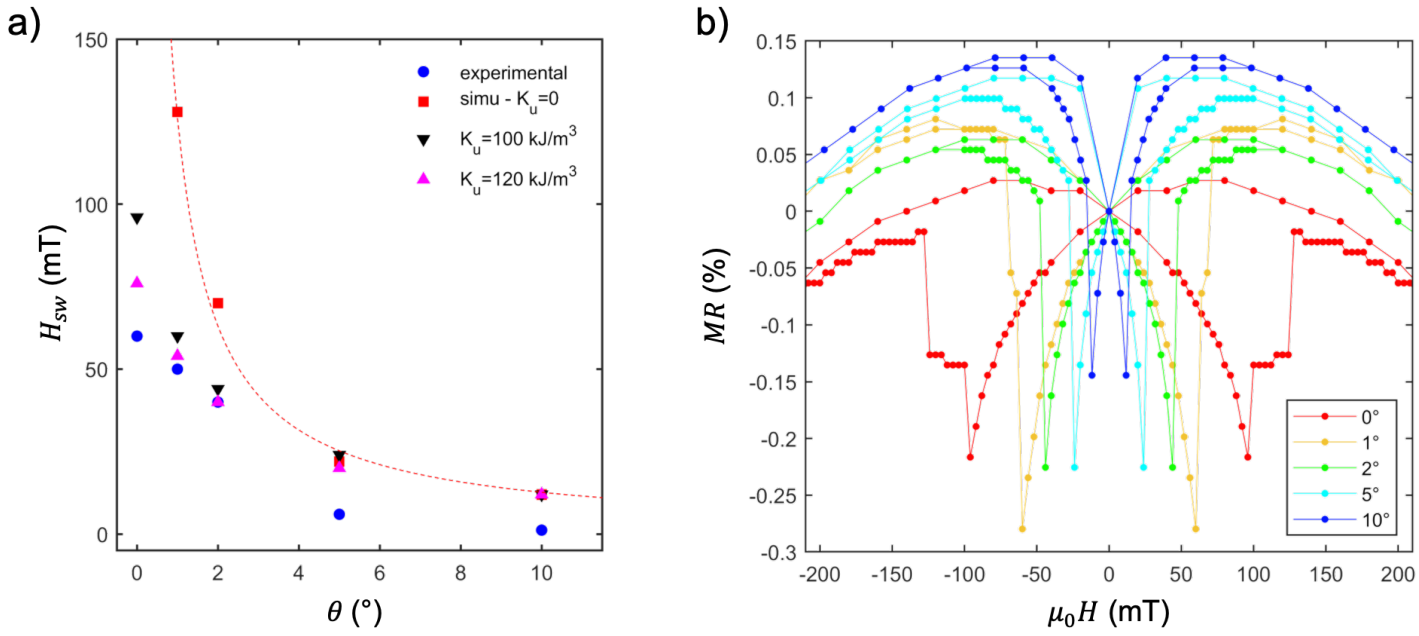

Figure 10: Numerical simulations of the magnetoresistance for a device with $t = 30$ nm and $w = 3$ μm including a tilted uniaxial magnetic anisotropy $\beta = 5.7°$. (a) Computed and experimental switching fields as a function of the misalignment angle for different intensity of anisotropy. (b) Magnetoresistance curves for different tilted external field for a device with $K_{u1} = 100$ kJ/m^3.

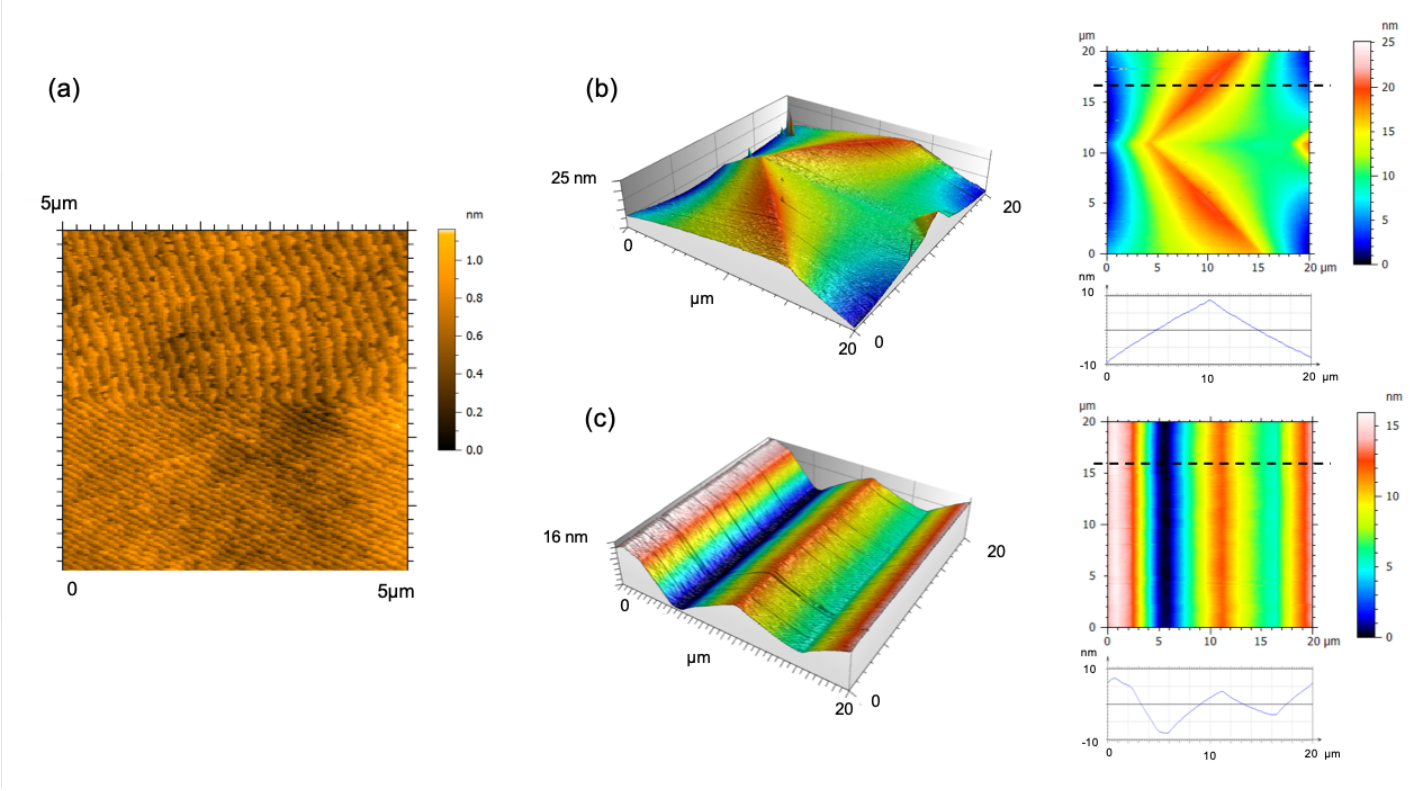

Figure 11: Topographic AFM images of a Py film of $t = 10$ nm grown on a LAO substrate obtained with different area scans. (a) A 5 μm x 5 μm image showing a twin boundary between two flat surfaces reproducing the substrate steps with a root mean square (rms) roughness of 0.13 nm. (b) and (c) Two 20 μm x 20 μm images where one can see that the twining structure of substrate is nicely reproduced in the thin film. Considering the twinning width (2 - 10 μm) and the height ($\sim$ 20 nm) one obtains an out-of-plain tilting twin angle of $\sim$ 0.1 - 0.5 °.

Table of Contents

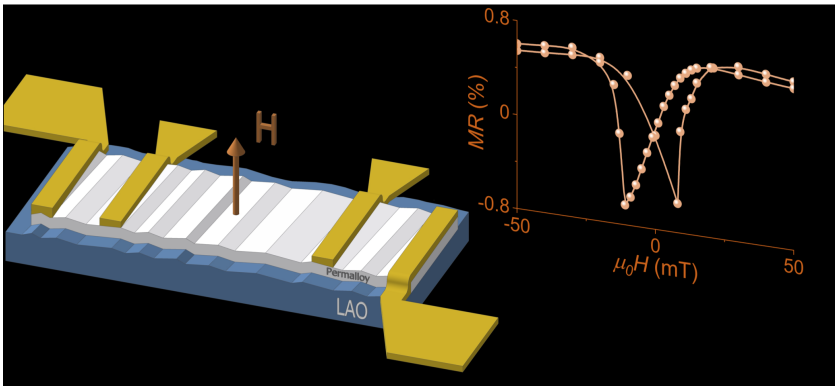

Permalloy strips with substrate-induced uniaxial anisotropy offer the possiblity to generate sharp magnetoresitanc changes triggered by low out-of plane magnetic fields. Sharp magnetization reversals tailored by the shape anisotropy of the strips are obtained potentially useful for sensing and advanced magnetoresistive devices.